Available online at www.sciencedirect.com
ScienceDirect
International Journal of Heat and Mass Transfer 50 (2007) 1892–1901
International Journal of HEAT and MASS TRANSFER
www.elsevier.com/locate/ijhmt

Steady natural convection flow in a square cavity filled with a porous medium for linearly heated side wall(s)

M. Sathiyamoorthy [a], Tanmay Basak [b], S. Roy [c], I. Pop [d,*]

[a] Department of Applied Mathematics, Birla Institute of Technology, Mesra, Ranchi 835 215, India
[b] Department of Chemical Engineering, Indian Institute of Technology Madras, Chennai 600 036, India
[c] Department of Mathematics, Indian Institute of Technology Madras, Chennai 600 036, India
[d] Faculty of Mathematics, University of Cluj, R-3400 Cluj, CP 253, Romania

Received 18 September 2006
Available online 6 December 2006

Abstract

In this paper natural convection flows in a square cavity filled with a porous matrix has been investigated numerically when the bottom wall is uniformly heated and vertical wall(s) are linearly heated whereas the top wall is well insulated. Darcy–Forchheimer model without the inertia term is used to simulate the momentum transfer in the porous medium. Penalty finite element method with bi-quadratic rectangular elements is used to solve the non-dimensional governing equations. Numerical results are presented for a range of parameters (Rayleigh number Ra, $10^3 \leqslant Ra \leqslant 10^6$, Darcy number Da, $10^{-5} \leqslant Da \leqslant 10^{-3}$, and Prandtl number Pr, $0.2 \leqslant Pr \leqslant 100$) in terms of stream functions and isotherm contours, and local and average Nusselt numbers.

Keywords: Penalty finite element method; Natural convection; Square cavity; Non-uniform heating

1. Introduction

Natural convection in fluid saturated porous media has received considerable attention over the last several years and non-Darcy effects on natural convection in porous media have a great deal of attention in recent years. This is due to a large number of technical applications, such as, fluid flow in geothermal reservoirs, separation processes in chemical industries, dispersion of chemical contaminants through water saturated soil, solidification of casting, migration of moisture in grain storage system, crude oil production, etc. Comprehensive literature survey concerned with this subject is given by Kaviany [1], Nield and Bejan [2], Ingham and Pop [3,4], Vafai [5,6], Pop and Ingham [7], Bejan and Kraus [8], Ingham et al. [9] and Bejan et al. [10].

The buoyancy driven convection in a porous cavity heated differentially in the horizontal side has been analyzed by Walker and Homsy [11] by a number of different techniques. The results obtained are fairly good agreement with each other as well as experimental results. The Brnikman-extended Darcy model has been considered by Tong and Subramanian [12], and Lauriat and Prasad [13] to examine the buoyancy effects on free convection in a vertical cavity. This model has been introduced by Brinkman [14] in order to account for the transition from Darcy flow to highly viscous flow (without porous matrix), in the limit of extremely high permeability. However, Brinkman model does not account adequately for the transition from porous medium flow to pure fluid flow as the permeability of the porous medium increases. A model that bridges the entire gap between the Darcy and Navier Stokes equations is the Darcy–Forchheimer model which was developed by Vafai and Tien [15]. It is known that the Darcy's law is an empirical formula relating the pressure gradient, the gravitational force and the bulk viscous resistance in porous media. Thus

* Corresponding author.
E-mail address: pop.ioan@yahoo.co.uk (I. Pop).

0017-9310/$ - see front matter © 2006 Elsevier Ltd. All rights reserved.
doi:10.1016/j.ijheatmasstransfer.2006.10.010

Nomenclature

Da	Darcy number
g	acceleration due to gravity, m s^{-2}
J	Jacobian of residual equations
k	thermal conductivity, W m^{-1} K^{-1}
K	permeability of the porous medium
L	side of the square cavity, m
Nu	local Nusselt number
p	pressure, Pa
P	dimensionless pressure
Pr	Prandtl number
Ra	Rayleigh number
T	temperature, K
T_h	temperature of hot bottom wall, K
T_c	temperature of cold vertical wall, K
u	x component of velocity
U	x component of dimensionless velocity
v	y component of velocity
V	y component of dimensionless velocity
X	dimensionless distance along x coordinate
Y	dimensionless distance along y coordinate

Greek symbols

α	thermal diffusivity, m^2 s^{-1}
β	volume expansion coefficient, K^{-1}
γ	penalty parameter
θ	dimensionless temperature
ν	kinematic viscosity, m^2 s^{-1}
ρ	density, kg m^{-3}
ψ	stream function

Subscripts

b	bottom wall
s	side wall

the mathematical formulations based on Dracy's law will neglect the effects of a solid boundary or the inertia forces on fluid flow and heat transfer through porous media. In general, the inertia and boundary effects become significant when the fluid velocity is high and the heat transfer is considered in the near wall region (see Chen and Lin [16]). In addition, the Darcy–Forchheimer model describes the effect of inertia as well as viscous forces in porous media and was used by Poulikakos and Bejan [17,18], Beckermann et al. [19], and Lauriat and Prasad [20] to examine the natural convection in a vertical porous layer and in a vertical enclosure filled with a porous medium. Further, natural convection in a square enclosure filled with a fluid saturated porous medium using a thermal non-equilibrium model has been investigated by Mohammad [21] for Brinkman-extended Darcy flow and by Baytas and Pop [22] for Darcy flow. Also, the effect of viscous dissipation has been considered for Darcy model by Saeid and Pop [23]. In contrast, very few investigations have been made in the past to focus on natural convection in porous medium due to uniform heating from below as reported by Basak et al. [24], Horne and O'sullivan [25], Caltagirone [26] and Straus [27].

The aim of the present investigation is to study a natural convective flow in a square cavity filled with a fluid saturated porous medium when the bottom wall is uniformly heated, left vertical wall is linearly heated and the right vertical wall is heated linearly or cooled while top wall is well insulated. The Darcy–Forchheimer model without the Forchheimer's inertia term has been adopted. In case of cooled right wall, the finite discontinuities in temperature distribution appear at the edges of the bottom wall. In our current study, we have used Galerkin finite element method with penalty parameter to solve the non-linear coupled partial differential equations governing flow and temperature fields. The momentum transfer in the porous medium is based on the Darcy–Forchheimer model. Numerical results are obtained to display the circulations and temperature distributions within the cavity and the heat transfer rate at the heated wall in terms of local and average Nusselt numbers.

2. Governing equations

Consider a fluid saturated porous medium enclosed in a square cavity of side L as shown in Fig. 1. The physical properties are assumed to be constant except the density in the buoyancy force term which is satisfied by the Boussinesq's approximation. Further, it is assumed that the temperature of the fluid phase is equal to the temperature of the solid phase everywhere in the porous region, and local thermal equilibrium (LTE) model is applicable in the present investigation [2]. Also, a velocity square term could be incorporated in the momentum equations to model the inertia effect which is more important for non-Darcy effect on the convective boundary layer flow over the surface of a body embedded in a high porosity media. However, we have neglected this term in the present study because we are dealing with the natural convection flow in a cavity filled with a porous medium. Under these assumptions and following Vafai and Tien [15] with the Forchheimer's inertia term neglected, the governing equations for steady two-dimensional natural convection flow in the porous cavity using conservation of mass, momentum and energy can be written as (see Du and Bilgen [29]):

$$\frac{\partial u}{\partial x}+\frac{\partial v}{\partial y}=0, \tag{1}$$

$$u\frac{\partial u}{\partial x}+v\frac{\partial u}{\partial y}=-\frac{1}{\rho}\frac{\partial p}{\partial x}+\nu\left(\frac{\partial^2 u}{\partial x^2}+\frac{\partial^2 u}{\partial y^2}\right)-\frac{\nu}{K}u, \tag{2}$$

$$u\frac{\partial v}{\partial x}+v\frac{\partial v}{\partial y}=-\frac{1}{\rho}\frac{\partial p}{\partial y}+\nu\left(\frac{\partial^2 v}{\partial x^2}+\frac{\partial^2 v}{\partial y^2}\right)-\frac{\nu}{K}v+g\beta(T-T_c), \tag{3}$$

$$u\frac{\partial T}{\partial x}+v\frac{\partial T}{\partial y}=\alpha\left(\frac{\partial^2 T}{\partial x^2}+\frac{\partial^2 T}{\partial y^2}\right) \tag{4}$$

with boundary conditions

$$\begin{aligned}
&u(x,0)=u(x,L)=u(0,y)=u(L,y)=0,\\
&v(x,0)=v(x,L)=v(0,y)=v(L,y)=0,\\
&T(x,0)=T_h,\quad \frac{\partial T}{\partial y}(x,L)=0,\quad 0<x<L,\\
&T(0,y)=T_h-(T_h-T_c)\frac{y}{L},\\
&T(L,y)=T_h-(T_h-T_c)\frac{y}{L}\quad \text{or}\quad T_c,
\end{aligned} \tag{5}$$

where x and y are the distances measured along the horizontal and vertical directions, respectively; u and v are the velocity components in the x- and y-directions, respectively; T denotes the temperature; ν and α are kinematic viscosity and thermal diffusivity, respectively; K is the medium permeability; p is the pressure and ρ is the density; T_h and T_c are the temperatures at hot bottom wall and cold vertical walls, respectively; L is the side of the square cavity. Using the following change of variables:

$$\begin{aligned}
&X=\frac{x}{L},\quad Y=\frac{y}{L},\quad U=\frac{uL}{\alpha},\quad V=\frac{vL}{\alpha},\quad \theta=\frac{T-T_c}{T_h-T_c},\\
&P=\frac{pL^2}{\rho\alpha^2},\quad Pr=\frac{\nu}{\alpha},\quad Da=\frac{K}{L^2},\quad Ra=\frac{g\beta(T_h-T_c)L^3Pr}{\nu^2},
\end{aligned} \tag{6}$$

the governing equations (1)–(4) reduce to non-dimensional form:

$$\frac{\partial U}{\partial X}+\frac{\partial V}{\partial Y}=0, \tag{7}$$

$$U\frac{\partial U}{\partial X}+V\frac{\partial U}{\partial Y}=-\frac{\partial P}{\partial X}+Pr\left(\frac{\partial^2 U}{\partial X^2}+\frac{\partial^2 U}{\partial Y^2}\right)-\frac{Pr}{Da}U, \tag{8}$$

$$U\frac{\partial V}{\partial X}+V\frac{\partial V}{\partial Y}=-\frac{\partial P}{\partial Y}+Pr\left(\frac{\partial^2 V}{\partial X^2}+\frac{\partial^2 V}{\partial Y^2}\right)-\frac{Pr}{Da}V+RaPr\theta, \tag{9}$$

$$U\frac{\partial \theta}{\partial X}+V\frac{\partial \theta}{\partial Y}=\frac{\partial^2 \theta}{\partial X^2}+\frac{\partial^2 \theta}{\partial Y^2} \tag{10}$$

with the boundary conditions

$$\begin{aligned}
&U(X,0)=U(X,1)=U(0,Y)=U(1,Y)=0,\\
&V(X,0)=V(X,1)=V(0,Y)=V(1,Y)=0,\\
&\theta(X,0)=1,\quad \frac{\partial \theta}{\partial Y}(X,1)=0,\\
&\theta(0,Y)=1-Y,\quad \theta(1,Y)=1-Y\quad \text{or}\quad \theta(1,Y)=0
\end{aligned} \tag{11}$$

Here X and Y are dimensionless coordinates varying along horizontal and vertical directions, respectively; U and V are dimensionless velocity components in the X- and Y-directions, respectively; θ is the dimensionless temperature; P is the dimensionless pressure; Ra, Pr and Da are Rayleigh, Prandtl and Darcy numbers, respectively.

3. Numerical method and choice of parameters

The momentum and energy balance equations (8)–(10) are solved using the Galerkin finite element method. The continuity equation (7) will be used as a constraint due to mass conservation and this constraint may be used to obtain the pressure distribution [30,31]. In order to solve Eqs. (8)–(10), we use the penalty finite element method where the pressure P is eliminated by a penalty parameter γ and the incompressibility criteria given by Eq. (7) (see Reddy [31]) which results in

$$P=-\gamma\left(\frac{\partial U}{\partial X}+\frac{\partial V}{\partial Y}\right). \tag{12}$$

The continuity equation (7) is automatically satisfied for large values of γ. Typical values of γ that yield consistent solutions are 10^7 [30,31].

Using Eq. (12), the momentum balance equations (8) and (9) reduce to

$$U\frac{\partial U}{\partial X}+V\frac{\partial U}{\partial Y}=\gamma\frac{\partial}{\partial X}\left(\frac{\partial U}{\partial X}+\frac{\partial V}{\partial Y}\right)+Pr\left(\frac{\partial^2 U}{\partial X^2}+\frac{\partial^2 U}{\partial Y^2}\right)-\frac{Pr}{Da}U, \tag{13}$$

and

$$U\frac{\partial V}{\partial X}+V\frac{\partial V}{\partial Y}=\gamma\frac{\partial}{\partial Y}\left(\frac{\partial U}{\partial X}+\frac{\partial V}{\partial Y}\right)+Pr\left(\frac{\partial^2 V}{\partial X^2}+\frac{\partial^2 V}{\partial Y^2}\right)-\frac{Pr}{Da}V+Ra\ Pr\ \theta. \tag{14}$$

The system of Eqs. (10), (13) and (14) with boundary conditions (Eq. (11)) is solved by using Galerkin finite element method. Since the solution procedure is explained in Ref. [24], the detailed description in not included in this paper. The numerical solutions are obtained in terms of the velocity components (U, V) and stream function (ψ) is evaluated using the relationship between the stream function (ψ) and the velocity components [32], where the stream function (ψ) is defined in the usual way as $U=\frac{\partial\psi}{\partial Y}$ and $V=-\frac{\partial\psi}{\partial X}$. It may be noted that the positive sign of ψ anti-clockwise circulation and the clockwise circulation is represented by the negative sign of ψ. The no-slip condition is valid at all boundaries as there is no cross flow, hence $\psi=0$ is used for the boundaries.

The heat transfer coefficient in terms of the local Nusselt number (Nu) is defined by

$$Nu=-\frac{\partial\theta}{\partial n}, \tag{15}$$

where n denotes the normal direction on a plane. The local Nusselt numbers at bottom wall (Nu_b) and at the vertical

walls (Nu_l, Nu_r) are evaluated for various wall boundary conditions, using above definition. The average Nusselt numbers at the bottom and side walls are computed as follows:

$$\overline{Nu_b} = \int_0^1 Nu_b \, dX, \quad \overline{Nu_l} = \int_0^1 Nu_l \, dY, \quad \text{and}$$
$$\overline{Nu_r} = \int_0^1 Nu_r \, dY. \tag{16}$$

The computational domain consists of 20×20 bi-quadratic elements which correspond to 41×41 grid points. The bi-quadratic elements with lesser number of nodes smoothly capture the non-linear variations of the field variables which are in contrast with finite difference/finite volume solutions available in the literature [12,20]. In order to assess the accuracy of our numerical procedure, we have tested our algorithm based on the grid size (41×41) for a square enclosure with a side wall heated and the results are in well agreement with the work of Lauriat and Prasad [20]. Comparisons are not shown here for the brevity of the manuscript.

Computations have been carried out for various values of $Ra = 10^3$–10^6, $Da = 10^{-5}$–10^{-3} and $Pr = 0.2$–100 with uniform bottom wall heating, linearly heated left wall and right wall is linearly heated or cooled where the top wall is well insulated. The jump discontinuities in Dirichlet type of wall boundary conditions at the corner points correspond to computational singularities. In particular, the singularity at the corner nodes of the bottom wall needs special attention. The grid size dependent effect of the temperature discontinuity at the corner points upon the local Nusselt numbers tend to increase as the mesh spacing at the corner is reduced. One of the ways for handling the problem is assuming the average temperature of the two walls at the corner and keeping the adjacent grid-nodes at the respective wall temperatures. In the current investigation, Gaussian quadrature based finite element method provides the smooth solutions at the interior domain including the corner regions as evaluation of residual depends on interior gauss points and thus the effect of corner nodes are less pronounced in the final solution. Since the detailed solution procedure is explained in a recent article [24], the description of the numerical method is omitted in the present manuscript. The present finite element approach offers special advantage on evaluation of local Nusselt number at the bottom and side walls as the element basis functions are used to evaluate the heat flux.

4. Results and discussion

4.1. Effect of Darcy number

4.1.1. Case I: Linearly heated side walls

Figs. 2–4 illustrate the stream function and isotherm contours of the numerical results for various $Ra = 10^3$–10^6, $Da = 10^{-5}$–10^{-3} and $Pr = 0.7$ when the bottom wall is uniformly heated and side walls are linearly heated where the top wall is well insulated. As expected due to linearly heated vertical wall and the uniformly heated bottom wall fluid rise up from middle portion of bottom wall and flow down along the vertical walls forming two symmetric rolls with clockwise and anti-clockwise rotations inside the cavity. In general, the fluid circulation is strongly dependent on Darcy number as can be seen in Figs. 2–4. Fig. 2 illustrates the stream function and temperature contours for $Da = 10^{-5}$ and $Ra = 10^6$, and the flow is seen to be very weak as observed from stream function contours. Therefore, the temperature distribution is similar to that with stationary fluid and the heat transfer is due to purely conduction. During conduction dominant heat transfer, the temperature $\theta \leqslant 0.3$ occur symmetrically near the top corners of the side walls in the enclosure. The other temperature $\theta \geqslant 0.4$ are smooth curves which span the entire enclosure and they are generally symmetric with respect to the vertical symmetric line.

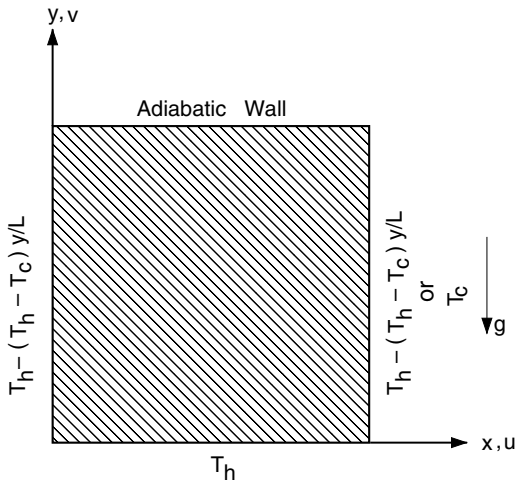

Fig. 1. Schematic diagram of the physical system.

As Darcy number increases to 10^{-4}, the strength of flow is increased at $Ra = 10^6$. The stronger circulation causes the temperature contours with $\theta = 0.5$ getting shifted towards the side wall and break into symmetric contour lines (see Fig. 3). Note that, at $Da = 10^{-4}$, the conduction dominant heat transfer mode would occur up to $Ra = 9 \times 10^4$. During $Da = 10^{-3}$, flow is a very strong function of Ra and the conduction dominant heat transfer occurs up to $Ra = 2 \times 10^4$. During conduction dominant mode, the temperature profile is similar to that in Fig. 2. The presence of significant convection is also exhibited in other temperature contours lines which start getting deformed and pushed towards the side wall. The conduction dominant heat transfer will be illustrated later via average Nusselt number vs. Rayleigh number plot and the critical Rayleigh number would demonstrate the significant effect of convective heat transfer.

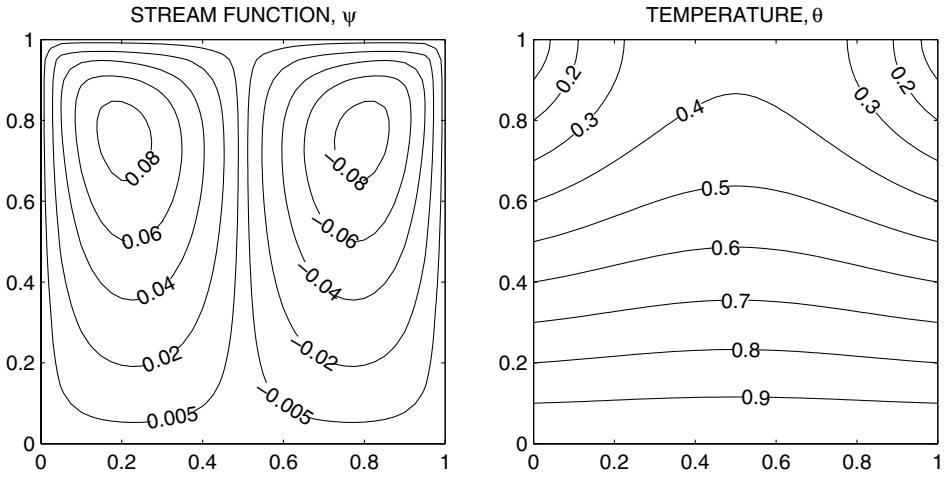

Fig. 2. Contour plots for linearly heated vertical walls $\theta(0, Y) = \theta(1, Y) = 1 - Y$, with $Pr = 0.7$, $Da = 10^{-5}$ and $Da = 10^{6}$. Clockwise and anti-clockwise flows are shown via negative and positive signs of stream functions, respectively.

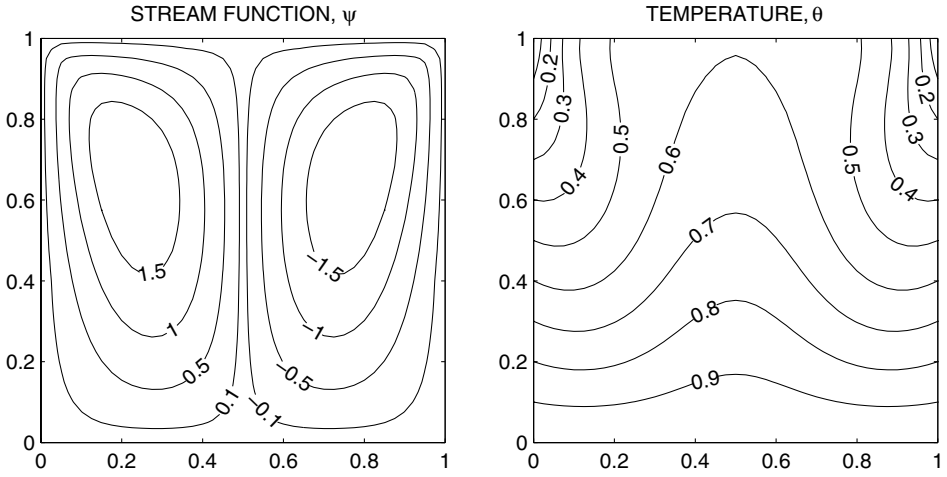

Fig. 3. Contour plots for linearly heated vertical walls $\theta(0, Y) = \theta(1, Y) = 1 - Y$, with $Pr = 0.7$, $Da = 10^{-4}$ and $Ra = 10^{6}$. Clockwise and anti-clockwise flows are shown via negative and positive signs of stream functions, respectively.

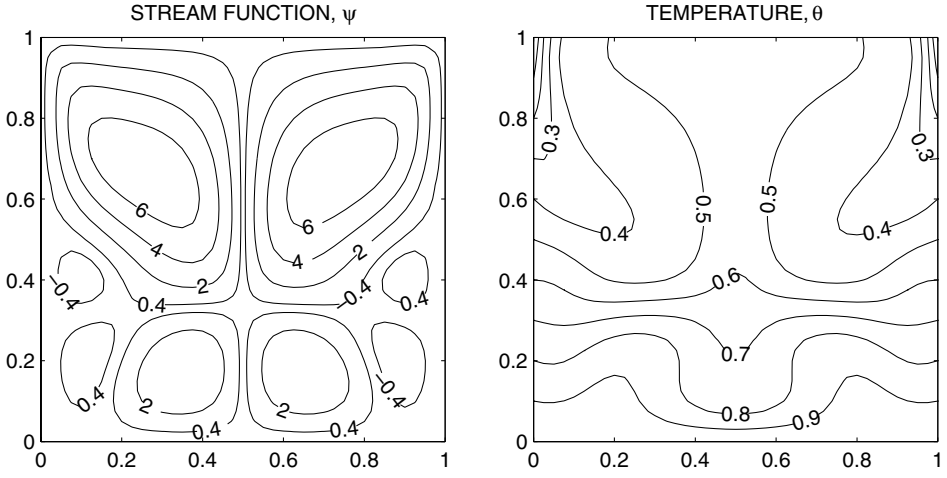

Fig. 4. Contour plots for linearly heated vertical walls $\theta(0, Y) = \theta(1, Y) = 1 - Y$ with $Pr = 0.7$, $Da = 10^{-3}$ and $Ra = 10^{6}$. Clockwise and anti-clockwise flows are shown via negative and positive signs of stream functions, respectively.

As Rayleigh number increases to 10^6 with $Da = 10^{-3}$, many secondary circulations appear at the bottom half of the cavity. The secondary circulations pushed the primary circulations towards the upper part of the cavity due to enhanced convection from the hot lower half of the cavity and hot fluid moves towards the center of cavity as seen from Fig. 4. The isotherm lines with greater values ($\theta \geqslant 0.5$) cover almost 80% of the cavity. It is interesting to observe that the pairs of symmetric circulations with 'hot' and 'cold' fluid regimes appear distinctly inside the cavity constituting the present natural convection flow. Comparative studies in Figs. 4–6 for a wide range of Prandtl number, Pr, from 0.2 to 1000 show many interesting features of stream function and isotherm contours in the cavity. The general trend is that higher Pr reduces the strength of secondary circulations while increases the strength of primary circulations (see Figs. 4–6). The physical reason is that higher Prandtl number fluid implies more viscous fluid which makes the secondary circulations weaker.

4.1.2. Case II: Linearly heated left wall with cooled right wall

Stream function and isotherm contours are displayed in Figs. 7–9 for $Da = 10^{-4}$–10^{-3}, $Ra = 10^6$ and $Pr = 0.2$–1000 with uniformly heated bottom wall, cooled right wall and the left wall is linearly heated. As expected due to linearly heated left wall, fluids rise up along the side of the left wall and flow down along the cooled right wall forming secondary circulations due to convection at the top corner of the left wall. Further, the hot fluid zone is created at the bottom corner of the left wall within the cavity. For $Da = 10^{-4}$ and $Pr = 0.7$, the temperature contours with $\theta = 0.5$ pushed towards the top corner of the left wall (see Fig. 7). At $Da = 10^{-3}$, the flow is stronger and the strength of the secondary circulation is increased and

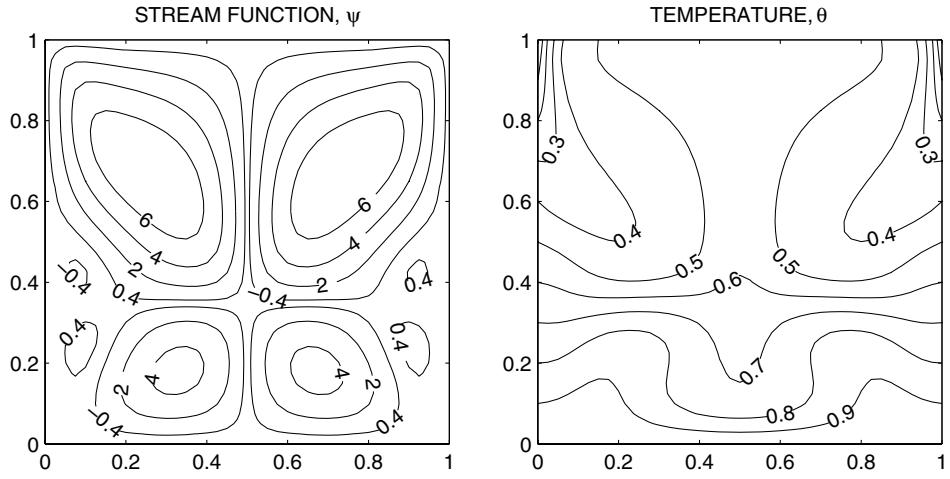

Fig. 5. Contour plots for linearly heated vertical walls, $\theta(0, Y) = \theta(1, Y) = 1 - Y$ with $Pr = 10$, $Da = 10^{-3}$ and $Ra = 10^6$. Clockwise and anti-clockwise flows are shown via negative and positive signs of stream functions, respectively.

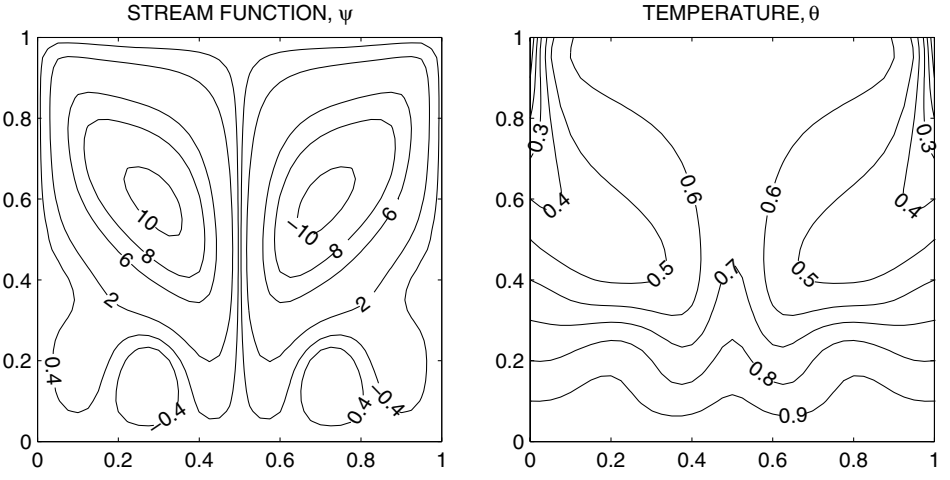

Fig. 6. Contour plots for linearly heated vertical walls, $\theta(0, Y) = \theta(1, Y) = 1 - Y$ with $Pr = 1000$, $Da = 10^{-3}$ and $Ra = 10^6$. Clockwise and anti-clockwise flows are shown via negative and positive signs of stream functions, respectively.

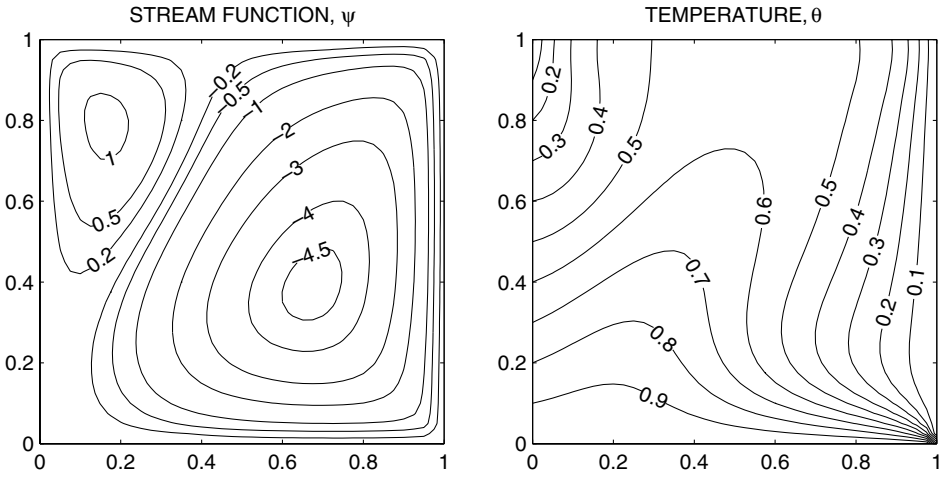

Fig. 7. Contour plots for linearly heated left vertical wall, $\theta(0, Y) = 1 - Y$ and cooled right vertical wall, $\theta(1, Y) = 0$, with $Pr = 0.7$, $Da = 10^{-4}$ and $Ra = 10^6$. Clockwise and anti-clockwise flows are shown via negative and positive signs of stream functions, respectively.

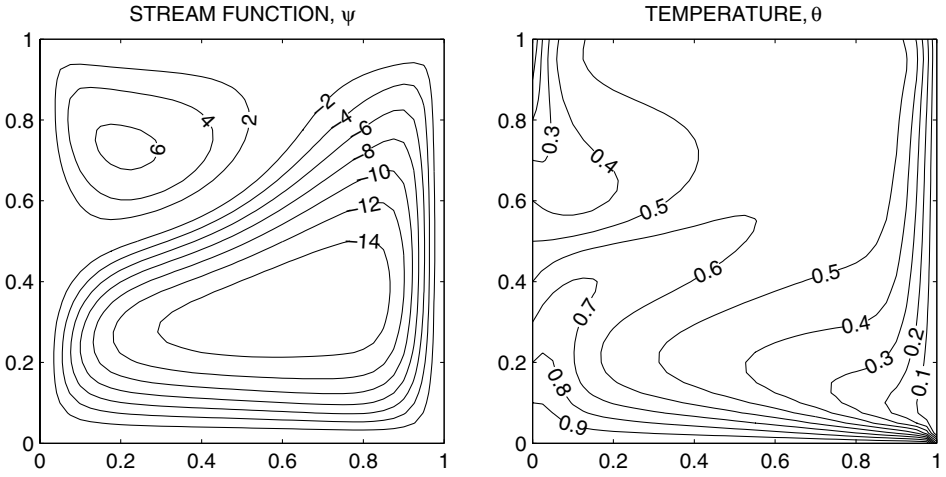

Fig. 8. Contour plots for linearly heated left vertical wall, $\theta(0, Y) = 1 - Y$ and cooled right vertical wall, $\theta(1, Y) = 0$, with $Pr = 0.7$, $Da = 10^{-3}$ and $Ra = 10^6$. Clockwise and anti-clockwise flows are shown via negative and positive signs of stream functions, respectively.

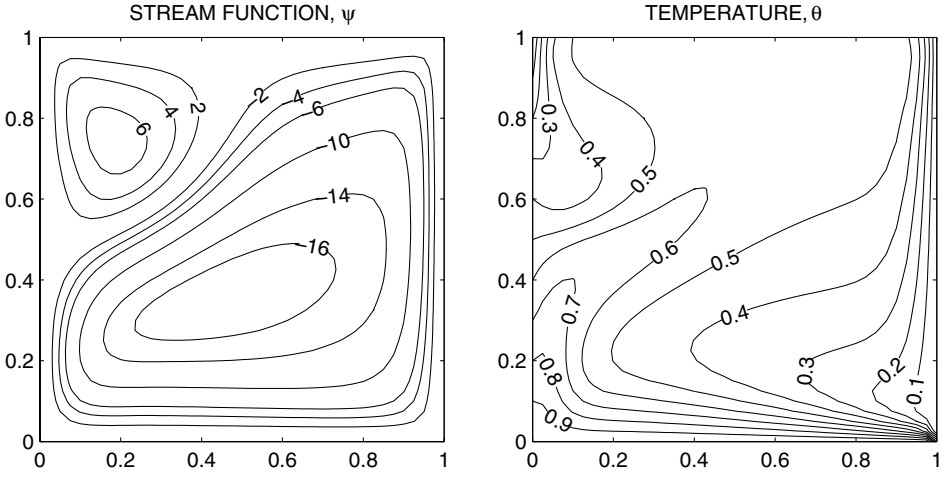

Fig. 9. Contour plots for linearly heated left vertical wall, $\theta(0, Y) = 1 - Y$ and cooled right vertical wall, $\theta(1, Y) = 0$, with $Pr = 1000$, $Da = 10^{-3}$ and $Ra = 10^6$. Clockwise and anti-clockwise flows are shown via negative and positive signs of stream functions, respectively.

pushed the primary circulation towards the right corner of the bottom wall. The isotherm contours with grater values $\theta \geqslant 0.5$ cover around 75% of the cavity. In this case for $Ra = 10^6$ and $Da = 10^{-3}$, comparative studies in Figs. 7–9 for the increase of Pr from 0.2 to 1000 do not show much significant change in the values of stream function and isotherm contours in the cavity except that the strength of the primary circulation increases slightly as shown in Fig. 9 for $Pr = 1000$. The significant effect of convective heat transfer will be illustrated via average Nusselt number vs. Rayleigh number plot in the next section.

4.2. Heat transfer rates: local and average Nusselt numbers

4.2.1. Case I: Linearly heated side walls

Fig. 10a and b displays the effect of Ra and Da on the local Nusselt numbers at the bottom and side walls (Nu_b, Nu_s) for $Pr = 0.7$ and 10. At the edges of the bottom wall, the heat transfer rate or Nu_b is 1 due to linearly heated side walls. For $Da = 10^{-4}$, the heat transfer rate is sinusoidal type with its minimum value at the center of the bottom wall due to higher values of stream function (i.e., flow rate)with two symmetric circulations about the vertical symmetric line at the center of the bottom wall. In contrast, for $Da = 10^{-3}$ at $Pr = 0.7$ and $Pr = 10$, the heat transfer rate is maximum at center of the bottom wall due to the presence of strong secondary circulation leading to hight temperature gradient at the center of bottom wall. It is observed in Fig. 10 that the local Nusselt number Nu_s is zero at the bottom-edge of the side wall due to uniformly heated bottom wall and it is maximum at the top-edges of side walls due to insulated top wall. For $Da = 10^{-5}$, $Pr = 0.7$, due to weak circulation, heat transfer rate is almost zero up to $Y = 0.7$ and $Nu_s = 3$ at $Y = 1$ whereas at Da^{-4}, the heat transfer rate $Nu_s = 5$ due to stronger circulations. For $Da = 10^{-3}$, due to the presence of a pair of symmetric secondary circulated cells with clockwise and anti-clockwise rotations, the heat transfer rate is oscillatory in nature and the increasing trend of heat transfer rate is observed in the upper half of the side walls with $Nu_s = 9$ and $Nu_s = 9.8$ at $Y = 1$ corresponding to $Pr = 0.7$ and 10, respectively.

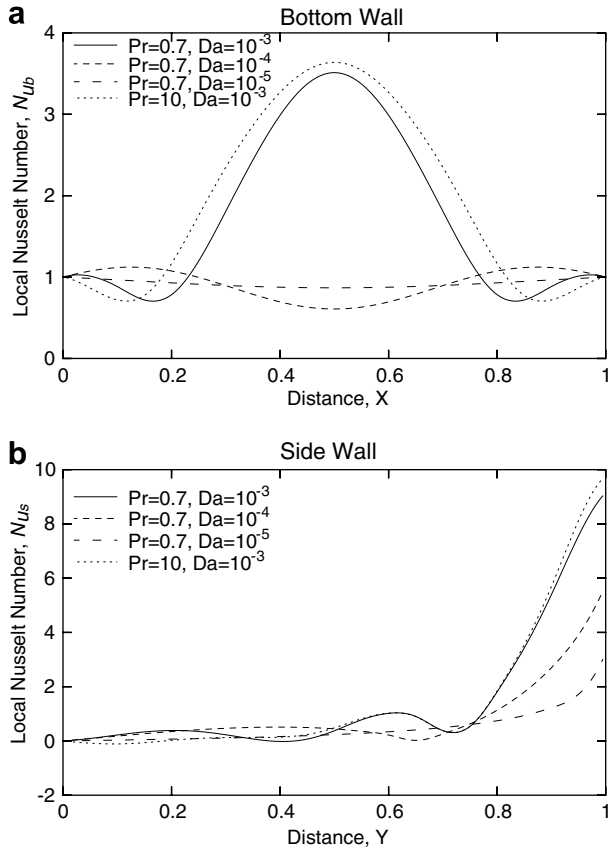

Fig. 10. Variation of local Nusselt number with distance at (a) bottom wall and (b) side wall for linearly heated side walls. The results are shown for $Ra = 10^6$.

The overall effects upon the heat transfer rates are displayed for linearly heated vertical walls in Fig. 12a and b, where the distributions of the average Nusselt number of bottom wall and vertical walls, respectively are plotted vs. the Rayleigh number. It is observed that the average Nusselt number is almost constant up to $Ra = 5 \times 10^5$ and $Ra = 7 \times 10^{-4}$ for $Da = 10^{-4}$ and $Da = 10^{-3}$, respectively due to dominant heat conduction mode and later smoothly increases with the increase of Rayleigh number further. It is interesting to note that, the smoothly increasing trend breaks at $Ra = 5 \times 10^5$ for $Pr = 0.7$ and $Da = 10^{-3}$ for both bottom and side walls due to the presence of strong multiple secondary cells. In contrast, for $Pr = 10$, the smoothly increasing trend of average Nusselt number with Ra is still observed due to the weak secondary cells for higher Prandtl numbers.

4.2.2. Case II: Linearly heated left wall with cooled right wall

Fig. 11a and b displays the effects of Da and Pr on local Nusselt numbers at the bottom and side walls (Nu_b, Nu_l, Nu_r) for linearly heated left wall and cooled right wall. The heat transfer rate Nu_b, is 1 at the left-edge of the bottom wall due to the linearly heated left wall and it is maximum at the right-edge of the bottom wall due to the cooled right wall (see Fig. 11a). As Da increases from 10^{-5} to 10^{-3}, the heat transfer rate increases everywhere at the bottom wall but for the increase of Pr from 0.7 to 10, there is a very little increase in heat transfer rate at the bottom wall. In Fig. 11b, the heat transfer rate (Nu_l) at the bottom-edge of the left wall is zero due to the uniformly heated bottom wall and linearly heated left wall and its magnitude increases from the bottom-edge to the top-edge of the left wall. At $Da = 10^{-3}$, local Nusselt number (Nu_l) exhibits oscillatory behavior due to the presence of secondary circulations near the top-edge of the left wall. The inset plot shows the local Nusselt number (Nu_r) distribution for the right wall. For all values of Da and Pr, it is observed that Nu_r is maximum at the bottom-edge and decreases towards the top-edge.

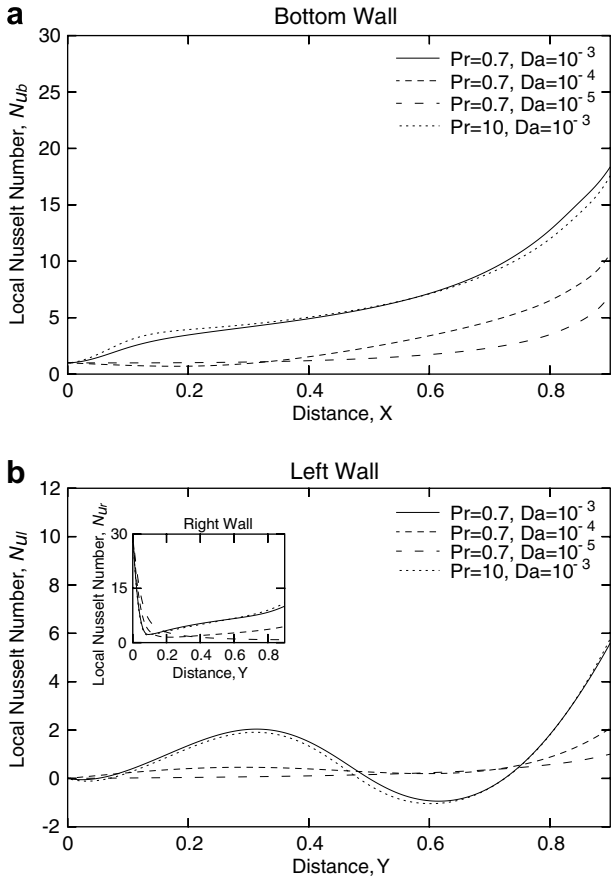

Fig. 11. Variation of local Nusselt number with distance at (a) bottom wall and (b) left and right walls for linearly heated left wall and cooled right wall. The results are shown for $Ra = 10^6$.

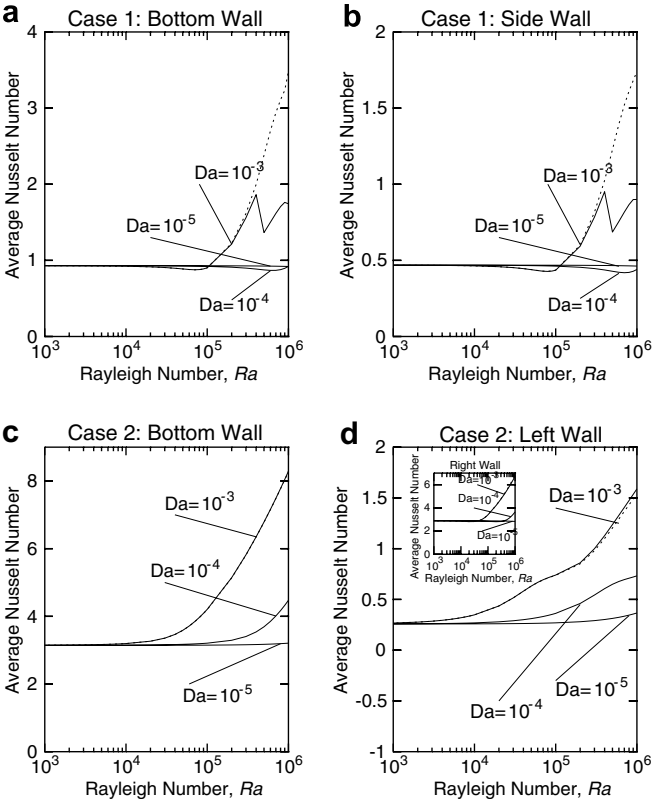

Fig. 12. Variation of average Nusselt number with Rayleigh number for linearly heated side walls [(a) and (b)] and linearly heated left wall and cooled right wall [(c) and (d)] with $Pr = 0.7$; (—) and $Pr = 10$: (---). The inset of d shows plot of average Nusselt number vs. Rayleigh number for right wall.

The overall effects of Ra, Pr and Da on the average Nusselt numbers at the bottom, left and right walls are displayed in Fig. 12c and d when the left vertical wall is linearly heated and right vertical wall is cooled while the bottom wall is uniformly heated. It is observed that the average Nusselt number of the bottom wall smoothly increases with the increase of Rayleigh number for $Da = 10^{-3}$ and $Da = 10^{-4}$ as seen in Fig. 12c. In contrast, variation of the average Nusselt number for the left wall does not show the unique trend for $Da = 10^{-4}$ and 10^{-3} due to secondary circulations appearing near the left wall. The inset of Fig. 12d shows the variation of average Nusselt number of right wall and the average Nusselt number is found to follow increase smoothly with Rayleigh number due to absence of multiple cells near the right wall. It is also interesting to note that the average Nusselt number for bottom and side walls seem to be negligibly influenced by Prandtl number.

5. Conclusions

The influence of linearly heated vertical wall(s) and uniformly heated bottom wall on flow and heat transfer characteristics due to natural convection within a square cavity filled with porous medium has been studied in the present investigation. The penalty finite element method helps to obtain smooth solutions in terms of stream function and isotherm contours for a range of Pr, Ra and Da. In case of linearly heated side walls, the presence of symmetric strong secondary circulations enhances the local mixing process in the lower half of the cavity for low Prandtl number fluid. Secondary circulations become weaker for higher Prandtl number fluid. The local Nusselt number exhibits oscillatory nature due to the presence of multiple secondary circulations. The average Nusselt numbers are almost constant in entire range of Ra up to 10^6 for $Da = 10^{-5}$ due to the conduction dominant mode of heat transfer but the average Nusselt number in general increases with the increase of Da and Ra. The effect of strong secondary circulation is also illustrated by the break in smoothness in average Nusselt number vs. Rayleigh number curve at $Ra = 5 \times 10^5$, $Pr = 0.7$ and $Da = 10^{-3}$. In case of linearly heated left wall, the oscillation in local Nusselt number occurs at the bottom wall due to secondary circulations at $Da = 10^{-3}$. Therefore, the average Nusselt number for the left wall also shows break in smoothness of the curve at high Ra and Da.

References

[1] S. Kaviany, Principles of Heat Transfer in Porous Media, Springer-Verlag, New York, 1995.

[2] D.A. Nield, A. Bejan, Convection in Porous Media, Springer-Verlag, New York, 1999.

[3] D.B. Ingham, I. Pop (Eds.), Transport Phenomena in Porous Media, vol. II, Pergamon, Oxford, 2002.

[4] D.B. Ingham, I. Pop (Eds.), Transport Phenomena in Porous Media, vol. III, Elsevier, Oxford, 2005.

[5] K. Vafai, Handbook of Porous Media, Marcel Dekker, New York, 2000.

[6] K. Vafai, Handbook of Porous Media, second ed., Taylor & Francis, New York, 2005.

[7] I. Pop, D.B. Ingham, Convective Heat Transfer, Mathematical and Computational Modeling of Viscous Fluids and Porous Media, Pergamon, Oxford, 2001.

[8] A. Bejan, A.D. Kraus (Eds.), Heat Transfer Handbook, Wiley, New York, 2003.

[9] D.B. Ingham, A. Bejan, E. Mamut, I. Pop (Eds.), Emerging Technologies and Techniques in Porous Media, Kluwer, Dordrecht, 2004.

[10] A. Bejan, I. Dincer, S. Lorente, A.F. Miguel, A.H. Reis, Porous and Complex Flow Structures in Modern Technologies, Springer, New York, 2004.

[11] K.L. Walker, G.M. Homsy, Convection in porous cavity, J. Fluid Mech. 87 (1978) 449–474.

[12] T.W. Tong, E. Subramanian, Boundary layer analysis for natural convection in porous enclosure: use of the Brinkman-extended Darcy model, Int. J. Heat Mass Transfer 28 (1985) 563–571.

[13] G. Lauriat, V. Prasad, Natural convection in a vertical porous cavity: a numerical study for Brinkman-extended Darcy formulation, Trans. ASME J. Heat Transfer 109 (1987) 295–320.

[14] H.C. Brinkman, On the permeability of media consisting of closely packed porous particles, Appl. Sci. Res. 1 (1947) 81–86.

[15] K. Vafai, C.L. Tien, Boundary and inertia effects on flow and heat transfer in porous media, Int. J. Heat Mass Transfer 24 (1981) 195–203.

[16] C.K. Chen, C.R. Lin, Natural convection from an isothermal vertical surface embedded in a thermally stratified high-porosity medium, Int. J. Eng. Sci. 33 (1995) 131–138.

[17] D. Poulikakos, A. Bejan, The departure from Darcy flow in natural convection in a vertical porous layer, Phys. Fluids 28 (1985) 3477–3484.

[18] D. Poulikakos, A departure from the Darcy model in boundary layer natural convection in a vertical porous layer with uniform heat flux, Trans. ASME J. Heat Transfer 107 (1985) 716–720.

[19] C. Beckermann, R. Viskanta, S. Ramadhyani, A numerical study of non-Darcdan natural convection in a vertical enclosure filled with a porous medium, Numer. Heat Transfer 10 (1986) 557–570.

[20] G. Lauriat, V. Prasad, Non-Darcian effects on natural convection in a vertical porous enclosure, Int. J. Heat Mass Transfer 32 (1989) 2135–2148.

[21] A.A. Mohammad, Non-equilibrium natural convection in a differentially heated cavity filled with a saturated porous matrix, Trans. ASME J. Heat Transfer 122 (2000) 380–384.

[22] A.C. Baytas, I. Pop, Free convection in a square porous cavity using a thermal non-equilibrium model, Int. J. Therm. Sci. 41 (2002) 861–870.

[23] N.H. Saeid, I. Pop, Viscous dissipation effects on free convection in a porous cavity, Int. Commun. Heat Mass Transfer 31 (2004) 723–732.

[24] T. Basak, S. Roy, T. Paul, I. Pop, Natural convection flow in a square cavity filled with porous medium: effects of various thermal boundary conditions, Int. J. Heat Mass Transfer 49 (2006) 1430–1441.

[25] R. Horne, M. O'sullivan, Oscillatory convection in a porous medium heated from below, J. Fluid Mech. 66 (1974) 339–352.

[26] J.P. Caltagirone, Thermoconvective instabilities in a horizontal porous layer, J. Fluid Mech. 72 (1975) 269–287.

[27] J.M. Straus, Large amplitude convection in porous media, J. Fluid Mech. 64 (1974) 51–63.

[29] Z.-G. Du, E. Bilgen, Natural convection in vertical cavities with internal heat generating porous medium, Wärme-und Stoffübertr 27 (1992) 149–155.

[30] T. Basak, K.G. Ayappa, Influence of internal convection during microwave thawing of cylinders, AIChE J. 47 (2001) 835–850.

[31] J.N. Reddy, An Introduction to the Finite Element Method, McGraw-Hill, New York, 1993.

[32] G.K. Batchelor, An Introduction to Fluid Dynamics, Cambridge University Press, 1993.